Shear Strength Prediction of High Performance Reinforced Concrete Deep Beams with Stirrups by ANSYS

Mohammad Ali Ihsan[1] & Omar Qarani Aziz[2] & Sinan Abdulkhaleq Yaseen[3]

[1,2,3] Civil Engineering Department, University of Salahaddin, Erbil, Iraq
Correspondence: Mohammad Ali Ihsan, University of Salahaddin, Erbil, Iraq.
Email: en.msaber@gmail.com

Received: June 16 , 2017 Accepted: August 28, 2017 Online Published: September 1, 2017

doi: 10.23918/eajse.v3i1sip212

Abstract: The present paper is a theoretical analyses of three dimensional (3D) finite element (FE) model to predicate the shear stress, shear strain, load deflection and crack propagation of sixteen high performance reinforced concrete deep beams (HPRCDB) with stirrups by ANSYS (v14). The main variables considered were; vertical shear stress ($\rho_v f_y$), ranging from 1.27 to 7.46MPa, horizontal shear stress ($\rho_h f_y$), ranging from 2.38 to 5.30 MPa and vertical and horizontal (combination) shear stress ($\rho_{vh} f_y$), ranging from (1.27+2.38 to 7.46+5.30) MPa, Three types of concrete were used based on the compressive strength; Normal Strength Concrete, (NSC), 43MPa, High Strength Concrete, (HSC), 62.5MPa, and High Performance Concrete, (HPC), more than 100MPa.Results obtained by ANSYS were compared with the experimental results in order to verify the accuracy of the finite element model. The theoretical results of the FE models show good agreement with the taken experimental data, in both linear and nonlinear behaviors ranges up to failure. The effect of each parameter were discussed and compared with the experimental works.

Keywords; ANSYS, Deep Beams, Finite Element, Shear Strength, High Performance

1. Introduction

Deep beam is defined as a structural member supported on one face and loaded on the opposite face, therefore compression struts will develop between the load and the supports (ACI 318M, 2014). Moreover, deep beams have either $(\frac{l_n}{h}) \leq 4.0$ (for distributed load case) or $(\frac{a}{d}) \leq 2.0$ (for points load case). Reinforced concrete deep beams appear as common structural elements in many structures starting from offshore gravity structures to high rise buildings. It is used as panel beam and, more recently, as deep grid wall in offshore gravity concrete structures. The term deep beam is applied to any beam has a depth to span ratio great enough to cause non-linearity in the elastic flexural stresses over the beam depth and the distribution of shear stress to be non-parabolic. The combination of stresses (bending and shear) in the shear span results inclined cracks which transform the beam into a tied-arch. In general reinforced concrete deep beams should have adequate shear reinforcement to prevent sudden and brittle failure after formation of the diagonal cracks, and also to keep crack width at an acceptable level. On the other hand, High Strength Concrete (HSC) is a concrete that has a specified design compressive strength of 55MPa or greater (ACI Committee 363, 2013). While, High Performance Concrete (HPC) is a concrete that meets special requirements of performance and uniformity in which cannot be achieved routinely using normal mixing, placing, and curing practices

and conventional constituent materials (ACI CT-13, 2013).

The ANSYS software has the ability of set up numerical models for the linear and nonlinear response of concrete element under both static and dynamic loading. In order to calibrate the initial finite element model a specific experimental test results were used. To create the FE model by ANSYS v14, there are numerous tasks should be complete for the model may run correctly. To create this model, the Graphical User Interface (GUI) was used. Solid65 (Eight-node solid brick) ANSYS elements were used to model the concrete, the elements contain a smeared crack similarity for tension zones cracking and to account the probability of concrete crushing in compression zone, it include a plasticity algorithm for that. Link180 ANSYS elements (3D spar elements) was used to model the flexural and shear stirrups reinforcement, these elements include elastic-plastic response of the reinforcing bars.

2. Finite Element Model

The present section all the FE modeling and analysis methods used for predicating the behavior of (HPRCDB) using ANSYS software, will be describe in detail.

3. Element Types

The following ANSYS element types were used to build the FE model:

3.1. Fiber Reinforced Concrete

The eight nodes Solid65 element with three degrees of freedom at each node, was used to modeling the concrete. The element has the ability of plastic deformation, cracking, and crushing in all three orthogonal directions. The steel fiber was modeled using the element Link 180 with smeared cracking method. Link 180 is a two node element with three degrees of freedom at each node, the element also having the ability of plastic deformation (Desayi & Krishnan,1964).

3.2. Reinforcement Bars

The two node elements Link180 (with three degrees of freedom, in all three orthogonal directions), was used to modeling all the reinforcement bars (flexural and shear stirrups). The element is also having the ability of plastic deformation (Desayi & Krishnan,1964).

3.3. Steel Fibers

Straight steel wire fibers (un-deformed) were used in this study. The fibers have aspect ratio (l/d) of (80), a nominal diameter of 0.2 mm and a nominal length of 40 mm. The Link180 element used to model the steel fibers.

3.4. Steel Plates

In order to avoid any localized crushing of concrete elements (Solid65), due to the problems of stress concentration near the load application points and supporting locations, thick steel baring plates (12.5 mm) was added at the support locations, to provide a more uniformly distribution for the stress over the support area. The steel plate was modeled using (Solid185) elements. Solid185

is an eight nodes element with three degrees of freedom at each node in x, y, and z directions (Desayi & Krishnan, 1964).

4. Material Properties

The concrete is assumed to be an isotropic and homogeneous material. It is a brittle material with two various behavior under compression and tension loads. An ideal stress-strain relationship for normal concrete is shown in Figure (1) (Bangash, 1989), this typical curve was not used for modeling the concrete in the FE material model, because, the negative slope part of the curve will cause convergence troubles. In order to obtain the uniaxial compressive stress strain curve for FE concrete model, the listed equations was used, to calculate the multi linear isotropic stress strain relationship for the concrete (Timoshenko & Gere, 1997).

$$f = \frac{E_c\,\varepsilon}{1+\left(\frac{\varepsilon}{\varepsilon_o}\right)^2} \qquad (1)$$

$$\varepsilon_o = \frac{2f_c'}{E_c} \qquad (2)$$

$$E_c = \frac{f}{\varepsilon} \qquad (3)$$

$f = Stress\ corsponding\ to\ any\ strain\ \varepsilon$
$\varepsilon = Strain\ corsponding\ to\ \ stress\ f$
$\varepsilon_o = Strain\ at\ ultimate\ compressive\ stress, f_c'$

The simplified uniaxial compressive stress strain curve that was used in this study is shown in Figure (2). The stress strain relationship for each deep beam model is built using six points linked by straight lines. The multi linear curve starts with zero stress strain point. The first Point (No.1) was computed at (0.40f'_c) stress, using Equation (3) from the linear stress-strain relationship of the concrete. Points No. 2, 3, and 4 were calculated from Equation (1), in which ε_0 is obtained from Equation (2). Point No. 5 is at ε_0 and f'_c. The stress strain relationship after Point No. 5 was assumed to be perfect plastic behavior.

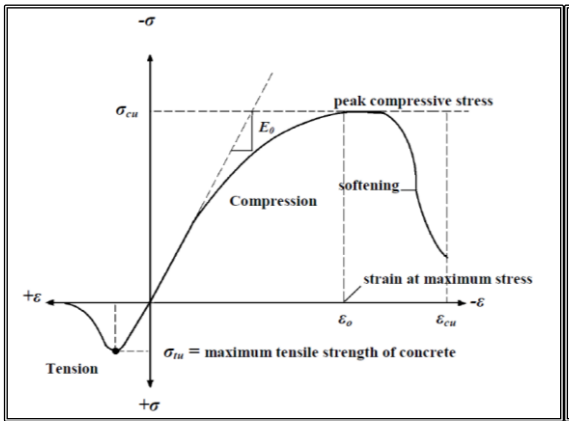

Figure (1): Typical Uniaxial Compressive and Tensile Stress Strain Curve for Concrete (Timoshenko & Gere, 1997)

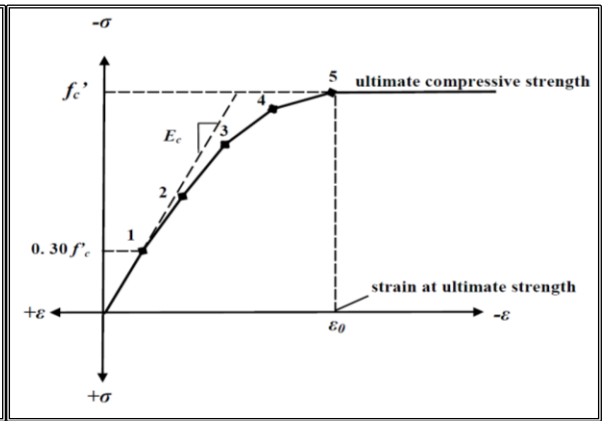

Figure (2): Simplified uniaxial compressive stress-stain relationship for concrete

5. Shear Reinforcement and Steel Plates

The stress-strain curve for the steel reinforcement used in the finite element model was obtained from the actual tensile tests.

6. Geometry and FE Modeling of HPC and Steel Reinforcement

The overall dimensions for all tested beams were 1250 mm long with an overall cross-section of 100x200 mm (effective depth d=167mm). All the tested specimens were simply supported over a clear span of 1000mm. The tested beams were divided into four groups. Figure (3) and Table (1), give the properties and details of the tested specimens (Aziz, 2015). In order to reduce the required time and disk size for computer computation process, only half of the full beam was used for modeling due to the symmetry of the tested beams.

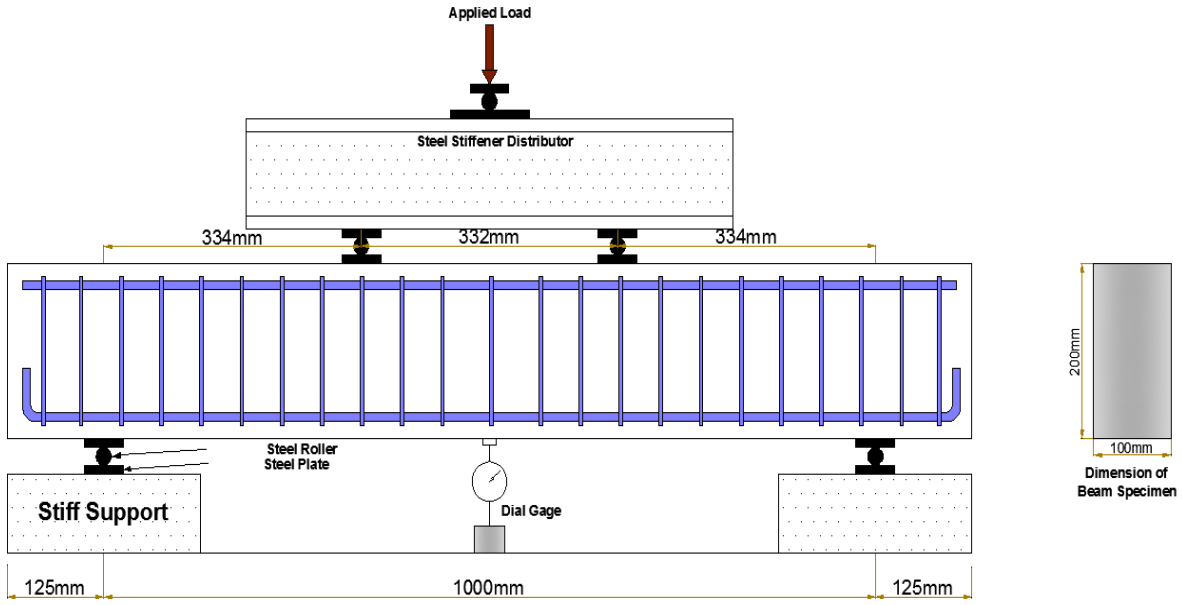

Figure (3): Detail of the Tested Specimens

Table (1): Detail of the Tested Specimens

Group No.	Beam designation	l/d	a/d	ρ_w %	fc` MPa	ρ_v fy MPa	ρ_h fy MPa
Group1	1. Bρvo	6.00	2.00	6.108	122	0.00	0.00
	2. Bρv1	6.00	2.00	6.108	122	1.27	0.00
	3. Bρv2	6.00	2.00	6.108	122	2.51,	0.00
	4. Bρv3	6.00	2.00	6.108	122	6.76	0.00
	5. Bρv4	6.00	2.00	6.108	118	7.46	0.00
Group2	6. Bρh1	6.00	2.00	6.108	118	0.00	2.38
	7. Bρh2	6.00	2.00	6.108	118	0.00	3.84
	8. Bρh3	6.00	2.00	6.108	118	0.00	5.30
Group3	9.Bρvh1	6.00	2.00	6.108	122.5	1.27	2.38
	10.Bρvh2	6.00	2.00	6.108	122.5	7.46	2.38
	11.Bρvh3	6.00	2.00	6.108	122.5	1.27	5.30
	12.Bρvh4	6.00	2.00	6.108	122.5	7.46	5.30
Group4	13. Bfc1	6.00	2.00	6.108	43	1.27	0.00
	14. Bfc2	6.00	2.00	6.108	62.5	1.27	0.00
	15. Bfc3	6.00	2.00	6.108	81	1.27	0.00
	16. Bfc4	6.00	2.00	6.108	99	1.27	0.00

7. Loading and Boundary Conditions

To get a unique solution, the model must be constrained using specific displacement boundary conditions. In order to enforce the model to behave as same way as the experimental tested specimens, boundary conditions must be applied at the symmetry loadings and supports locations. First the boundary conditions for symmetry were set. The model is one plane symmetric model. Figure (4), shows all the applied boundary conditions for planes of symmetry and end supports. The section in which defines the plane of symmetry is a vertical plane through center of the beam at mid-span. In order model the symmetry condition, all nodes in plane of symmetry, restrained in the longitudinal direction. Therefore the displacement along the X-direction for all the nodes in this plane were equaled to zero, (UX = 0). The end support was modeled as a roller support. A set of nodes on a single line of the steel plate element were restrained in the Y and Z directions, by gave constant values of zero (UY=0, UZ=0), so as, the beam will be free to rotate at the support. The applied load, P, is applied a cross all the entire nodes of the steel plate.

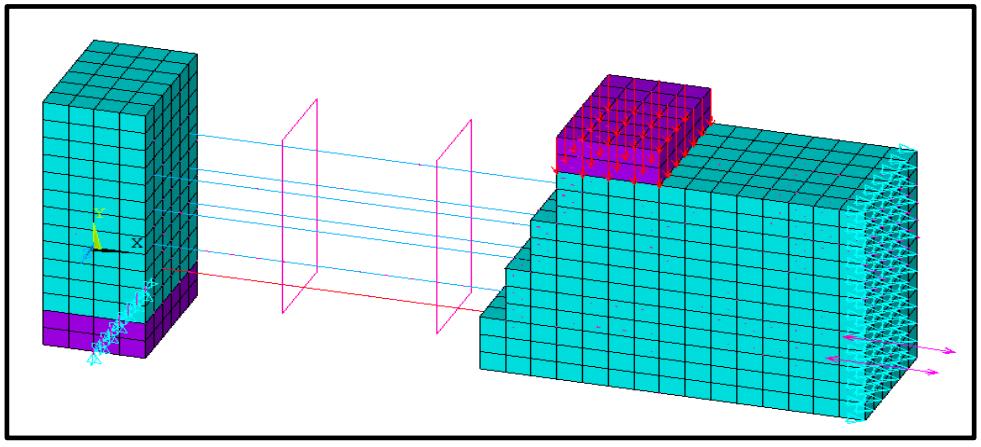

Figure (4): Typical Steel Reinforcement Locations for the Half-Size Beams

8. Predicted Results from the FE Model

The results from the ANSYS-FEM include the following:

1. Ultimate load capacity and failure modes.
2. Ultimate shear stress and strain distribution.
3. First shear and flexural cracking loads.
4. Load Deflection curve.
5. Pattern of Cracks propagating.

9. Ultimate Load Capacity (Failure load)

The theoretical ultimate load capacity (which was considered as the last converged load in the FEM analysis) and mode of failure for all tested beams are shown in Table (2). The predicted load shows good agreement compared with the experimental results. The overall percentage of experimental to the predicated (ANSYS model) load ratio is with (99%), Table (5). Which indicate the perfect calibration of the FE-ANSYS model to perform such simulations close to the reality.

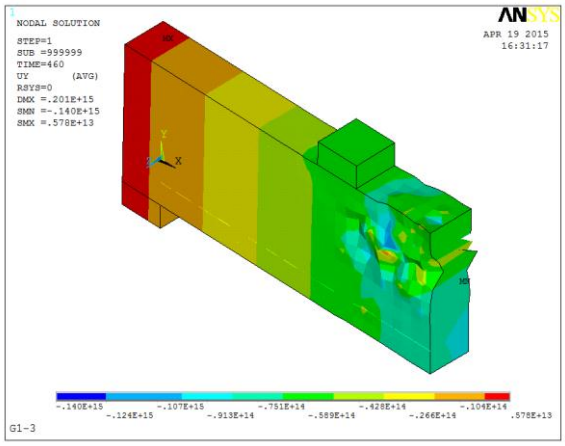

Figure (5): Shear Compressive Failure Mode

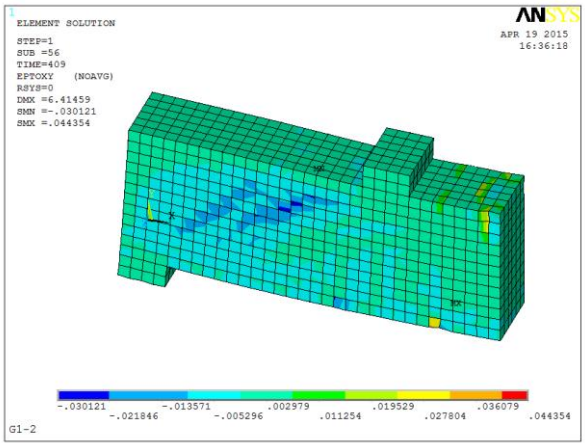

Figure (6): Diagonal Tension Failure Mode

10. Maximum Shear Stress and Strain Intensity

The maximum shear stress for all tested beams shown in Table (2). In which was considered as the (XY) shear stress at the last converged iteration before failure. The overall theoretical results were higher than those from experimental work by approximately 20%. The stress distribution across the beams side surface for beam specimen (G3-1), shown in Figure (7), with maximum shear stress of (16.54 MPa). The strain intensity for beam specimen (G3-1), shown in Figure (8) in which the diagonal tension failure is clear to be happen.

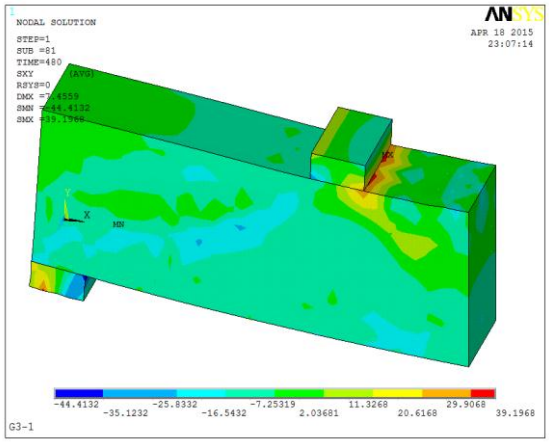

Figure (7): Shear Stress Distribution for Beam (G3-1)

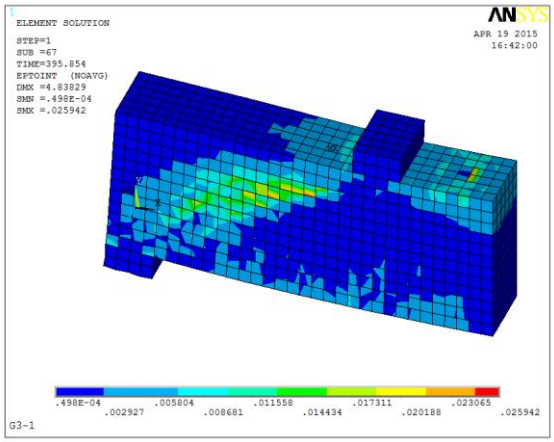

Figure (8): Strain Intensity for Beam (3-1)

Table (2): Experimental and Predicted, First Cracking Load, Ultimate Load Capacity, Ultimate Shear Stress and Mode of Failure for All Tested Specimens

Beam No.	Experimental First Flexural Cracking Load MPa	Predicted First Flexural Cracking Load MPa	% (Experimental/Predicted) First Flexural Cracking Load	Experimental First Shear Cracking Load MPa	Predicted First Shear Cracking Load MPa	% (Experimental/Predicted) First Shear Cracking Load	Experimental Failure Load (kN)	Predicted Failure Load (kN)	% (Experimental/Predicted) Failure Load	Experimental Ultimate Shear Stress MPa	Predicted Ultimate Shear Stress MPa	% (Experimental/Predicted) Ultimate Shear Stress	Experimental Mode of Failure	Predicted Mode of Failure
G1-1	57	36.9	154	161	101.	159	319	320	100	9.55	10.3	92	Diagonal Tension	Diagonal Tension
G1-2	60	42.6	141	182	122.	148	430	420	102	12.874	14.0	92	Diagonal Tension	Diagonal Tension
G1-3	65	44.2	147	195	125.	155	460	460	100	13.77	16.0	86	Diagonal Tension	Shear
G1-4	68	45.6	149	240	136.	176	489	488	100	14.64	20.4	72	Shear	Shear
G1-5	67	45.8	146	240	132.	181	500	500	100	14.97	23.1	65	Shear	Shear
G2-1	64	43.5	147	175	105.	166	410	409	100	12.275	17.6	69	Diagonal Tension	Diagonal Tension
G2-2	63	44.2	143	185	120.	154	440	440	100	13.174	19.9	66	Diagonal Tension	Diagonal Tension
G2-3	62	44.8	138	205	122.	168	460	460	100	13.772	20.8	66	Diagonal Tension	Diagonal Tension
G3-1	64	48.5	132	195	135.	144	450	480	94	13.473	16.5	81	Diagonal Tension	Diagonal Tension
G3-2	66	47.8	138	216	148.	145	542	540	100	16.2	17.2	94	Diagonal Tension	Shear
G3-3	64	49.2	130	230	165.	139	520	560	93	15.8	16.4	96	Shear	Shear
G3-4	68	28.6	238	245	187.	131	560	578	97	16.766	18.2	92	Shear	Shear
G4-1	44	24.6	179	70	36.5	192	190	184	103	5.7	8.2	70	Diagonal Tension	Diagonal Tension
G4-2	47	28.8	163	132	45.2	292	313	321	98	9.37	12.4	76	Diagonal Tension	Diagonal Tension
G4-3	50	32.8	152	178	78.5	227	384	392	98	11.5	13.4	86	Diagonal Tension	Diagonal Tension
G4-4	55	37.8	146	195	104.	187	400	418	96	12	14.2	84	Diagonal Tension	Shear
	Average		153			173			99			80		

11. First Cracking Load

The theoretically first (shear or flexural) cracking load is the load stage when the first cracking signs is taken place in concrete elements (solid65). The cracking load for all test beams have been compared with those form experimental results, Table (5). The experimental to the predicted results ratio is within an average of (153% for shear and 173% for flexural). Mostly the load of first crack

obtained from the ANSYS model is lower than from experimental results. This is due to the fact that the experimental cracking load is the load where the first visible crack (shear or flexural) appear, while the theoretical cracking load is the load step where one of the principal stress in concrete element reach the maximum limit.

12. Load-Deflection Curves

Theoretical (FEM-ANSYS) and the experimental *mid span deflection* is calculated and obtained form same location on the tested beam. The load deflection curves from the FEM and the experimental results for beam specimen (G1-2) and (G2-3) are shown in Figure (9) and (10) respectively. The predicted load-deflection curves shows good agreement with that from experimental work, although, it was more stiffener in all loading stages. Mostly because of:

1. For pre-cracking stages (before cracking): the first cracking loads calculated by the FE-ANSYS model were greater than those from the experimental results.
2. For post-cracking stages: micro-cracks formed by drying shrinkage and handling are existing in the real concrete. This would lead to reducing the stiffness of the actual beams, while in the FE models such micro-cracks do not include. And the ideal assumed bond between the concrete and reinforcement bar in FEM, while these assumptions would not be exist in real concrete beams.

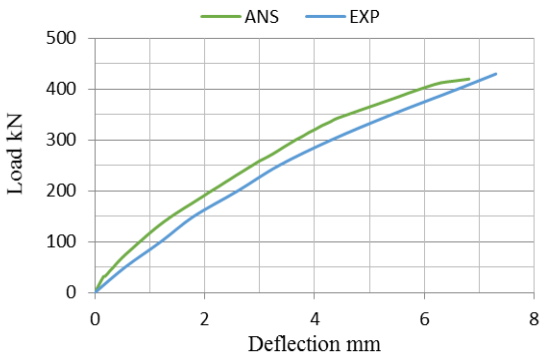

Figure (9) Experimental and Predicted Load Deflection Curve For Beam G1-2

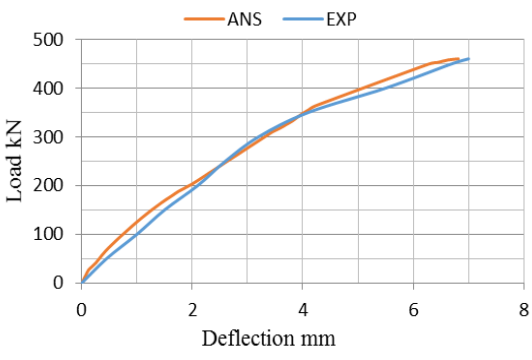

Figure (10) Experimental and Predicted Load Deflection Curve For Beam G2-3

13. Crack Pattern

For all applied load stages, ANSYS software records the crack pattern. When the principal tensile stress value for Solid65 element exceeds the concrete ultimate tensile strength a cracking sign performed and a circle shape appears. The direction of the appeared cracking sign is perpendicular to the direction of principal stress. Generally, at early loading stages flexural cracks appears at mid span. By increasing the applied loads, the flexural cracks propagate horizontally from the mid span towards the support. At a higher level of loading stages, diagonal tensile cracks perform. Additional flexural and diagonal tensile cracks appears with increasing the applied loads. No compressive cracks performed under or near the loading location, as the model is for deep beam. An example of the predicted crack pattern is shown in Figure (11) and (12). This pattern was obtained from the solution of the beams specimen (G1-5). The amount of cracks shown in the Figure (11) and (12) from FE-ANSYS model analysis is much more than what is observed in the experimental test. In FE model, maximum three cracks can be predicted for each Solid65 element. Therefore, the total

number of the predicted cracks in FE model is a function of used mesh size. So using a larger size for Solid65 elements mesh lead to fewer amount of elements and less number of cracks appears; and vice versa. It is better to consider the appeared cracks as contours of where the principal tensile stresses exceeds the ultimate tensile strength of concrete.

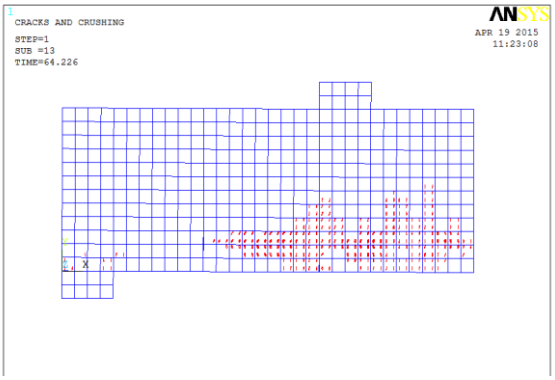

Figure (11) Flexural Crack Pattern for Beam (G1-5)

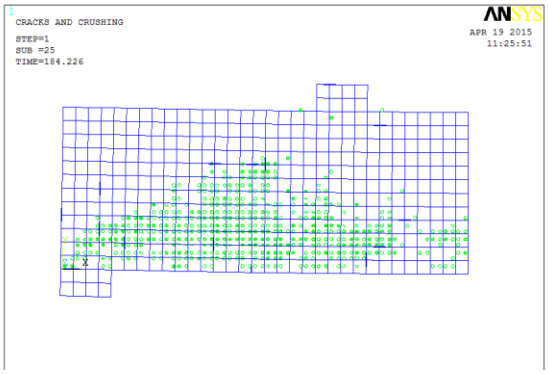

Figure (12) Shear Crack Pattern for Beam (G1-5)

14. Conclusion

1. The predicted ultimate final deflection, load-deflection curves and mode of failure by the FE model, show good agreement with the experimental data.
2. Effect of additional variables on the shear behavior HPRCDB such as, loading type, the value of $\left(\frac{a}{d}\right)$, and main reinforcement ratio.
3. The (Experimental/Predicted) failure load for all the tested beams were within (99%), while the FEM beams seem stiffer than the experimental beams during the loading, this fact due to the absent of micro cracks in the FE model and the perfect bond assumption between the concrete and reinforcement bar.
4. First (shear and flexural) cracking load predicted by FE model for all the tested beams was lower than those from experimental works tests by (153% for shear and 173% for flexural), the experimental first cracking load is the load where the first visible crack (shear or flexural) appear, while the theoretical cracking load is the load step where one of the principal stress in concrete element reach the maximum limit.
5. The number of cracks in the FE model is much more than observed in the experimental test, since the number of cracks appeared is a function of the used mesh size.
6. The predicted crack pattern can be consider as contours of wherever the principal tensile stress exceeds the ultimate tensile strength of concrete, rather than as indication of number of cracks, crack spacing or cracks width.
7. The predicted ultimate shear stresses were higher than those from experimental work by approximately 20% for all tested beams.
8. The predicted shear stress intensity from the FEM can be used to study the shear stress distribution along the deep beam depth in various loading stages.

References

ACI 318M (2014). *Building Code Requirements for Structural Concrete and Commentary*, reported by ACI committee 318.

ACI Committee 363 (2013). *State of the Art Report on High Strength Concrete*, ACI Manual of Concrete Practice, Part 5.

ACI CT-13 (2013). *ACI Concrete Terminology*, ACI STANDARD, First Printing January 2013.

ANSYS User's Manual Revision (2011). ANSYS. Inc., Canonsburg, Pennsylvania.

Aziz, O. Q. (2015). Experimental Investigation on Shear Strength of High Performance Reinforced Concrete Deep Beams with Stirrups, *Proceeding of 2nd ICEEE*, Erbil.

Bangash, M. Y. H. (1989). *Concrete and Concrete Structures: Numerical Modeling and Applications*. London: Elsevier Science Publishers Ltd.

Desayi, P., & Krishnan, S. (1964). Equation for the Stress-Strain Curve of Concrete. Journal of the American Concrete Institute, 61(3), 345-350.

Timoshenko, S. P. & Gere J. M. (1997). *Mechanics of Materials*. Boston: PWS Publishing Company.

Nilson, H., & Darwin, D. (2004). *Design of Concrete Structures. International Edition*, 13th edition.